Nano Energy 88 (2021) 106287

Contents lists available at ScienceDirect

Nano Energy

journal homepage: www.elsevier.com/locate/nanoen

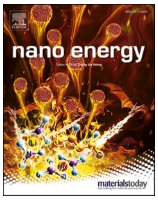

Triboelectric plasma decomposition of CO_2 at room temperature driven by mechanical energy

Sumin Li [a,1], Bao Zhang [a,1], Guangqin Gu [a], Xiaochen Xiang [a], Wenhe Zhang [a], Xue Shi [a], Ke Zhao [a], Yifei Zhu [b], Junmeng Guo [a], Peng Cui [a], Gang Cheng [a,*], Zuliang Du [a,*]

[a] *Key Lab for Special Functional Materials, Ministry of Education, National & Local Joint Engineering Research Center for High-efficiency Display and Lighting Technology, School of Materials Science and Engineering, and Collaborative Innovation Center of Nano Functional Materials and Applications, Henan University, Kaifeng 475004, China*

[b] *Institute of Aero-engine, School of Mechanical Engineering, Xi'an Jiaotong University, Xi'an 710049, China*

ARTICLE INFO

Keywords:
Triboelectric nanogenerator
Triboelectric plasma
CO_2 decomposition
CO_2^- reactive species
Electron attachment dissociation

ABSTRACT

CO_2 conversion into high value-added chemicals and fuels has received considerable attention. However, the direct decomposition of CO_2 using mechanical energy, which is an important renewable energy, remains challenging. This study realized triboelectric plasma decomposition of CO_2 into CO with near 100% selectivity under normal temperature and pressure, which could be directly driven by mechanical energy. CO_2^- reactive species were detected by electron paramagnetic resonance spectra, verifying the existence of electron attachment dissociation (EAD) process of CO_2 with a lower dissociation barrier. Average electron energy in the triboelectric plasma was decreased by modulating the distance and the polarity; thus, EAD proportion in the CO_2 decomposition was increased, and a maximum CO evaluation rate of 2.2 μmol h^{-1} and an energy efficiency of 5.2% from plasma to chemical energy were achieved. This work provides a promising strategy for CO_2 decomposition using mechanical energy.

1. Introduction

While fossil fuels supply large amounts of energy for the modern society, their burning directly emits a large amount of greenhouse gases, specifically carbon dioxide (CO_2), produced in the industrial exhaust, automobile exhaust etc., which has caused an increasingly serious environmental crisis worldwide [1,2]. As one of the most important ways of solving this crisis, decomposing CO_2 and converting it into high value-added chemicals have attracted widespread attention from researchers. The direct thermal decomposition of CO_2 into CO is still a mainstream method for CO_2 conversion [3–5]. Owing to the strong thermodynamic stability of CO_2, its direct thermal decomposition must be achieved at a high temperature above 2000 K, increasing its cost [6–8]. Moreover, the energy consumed by high-temperature heating is mostly supplied from fossil fuels, and these processes still emit CO_2, which makes it difficult for thermal decomposition to fundamentally solve the problem of CO_2 emission reduction [9]. Therefore, directly using renewable energy to efficiently convert CO_2 into chemical feedstock or fuel is an ideal strategy for achieving a green and sustainable CO_2 recovery [10,11].

Mechanical energy is a green and cheap renewable energy that is widely available in nature. It has many forms, including wind, tide, hydropower, and ocean wave [12–18]. Triboelectric nanogenerator (TENG) is now becoming an emerging technology that converts mechanical energy into electrical energy and can efficiently collect irregular mechanical energy that widely exists in nature [19–23]. TENG is characterized with high voltages, which can directly breakdown the gas and produce plasma [24–27]. The high-energy electrons in plasma can interact with chemical molecules, forming highly reactive species or directly breaking chemical bonds. Therefore, plasma is endowed with an outstanding technical advantage in decomposing highly stable molecules, such as CO_2 and N_2 [28,29]. For example, plasma technology has been successfully applied in CO_2 decomposition and the selectivity for the direct decomposition of CO_2 into CO is low [30,31]. However, traditional plasma technology requires complex plasma generators and a sophisticated electrical control system. More importantly, it cannot be directly driven by renewable mechanical energy [32]. The plasma powered by a TENG, which is called a triboelectric plasma, was recently

---

[*] Corresponding authors.
E-mail addresses: chenggang@henu.edu.cn (G. Cheng), zld@henu.edu.cn (Z. Du).

[1] These authors contributed equally to this work.

https://doi.org/10.1016/j.nanoen.2021.106287
Received 20 April 2021; Received in revised form 3 June 2021; Accepted 22 June 2021

applied in the reaction of converting nitrogen into nitrogen oxide compounds, achieving atmospheric nitrogen fixation [33,34]. Triboelectric plasma is directly driven by the widely distributed and effectively utilized renewable mechanical energy in nature, which is a low-cost, effective, and simple system for generating plasma over a wide range of conditions [25,35]. Hence, it is highly desirable to decompose CO_2 molecules through triboelectric plasma by utilizing renewable mechanical energy.

This study designed triboelectric plasma with a needle-plate discharge configuration to realize CO_2 decomposition into CO with near 100% selectivity under room temperature and normal pressure conditions. Electron paramagnetic resonance (EPR) showed that highly reactive CO_2^- anions were produced during the decomposition process. The decomposition barrier of CO_2^- anions was calculated as 3.7 eV lower than that of neutral CO_2 molecules, which can effectively improve the activity and energy efficiency of CO_2 decomposition. The average energy of electrons in the triboelectric plasma could be reduced by regulating the needle-plate distance and corona discharge polarity, which was advantageous to the generation of highly reactive CO_2^- anions. The needle-plate distance (***d***) was 1.5 mm; thus, the CO_2 decomposition to CO rate in negative corona was 2.2 μmol h^{-1}, and a record energy efficiency from mechanical energy to chemical energy was 1.2%. Finally, the triboelectric plasma driven by 4.7 m s^{-1} wind was demonstrated to dramatically decompose CO_2. This work provides a novel, sustainable, and environment-friendly strategy for converting CO_2 into high value-added chemicals by utilizing mechanical energy.

2. Results and discussion

2.1. *Triboelectric plasma CO_2 decomposition system driven by mechanical energy*

The triboelectric plasma CO_2 decomposition system mainly includes three parts, that is, a TENG, a gas reactor, and an electrical test system (Figs. 1a and S1). When the polytetrafluoroethylene (PTFE) comes into contact with metallic copper, negative tribo-charges are formed on the PTFE surface, and metallic copper is positively charged. As the PTFE rotates, an alternating current output is generated in the external circuit transformed into a direct current output through a full-wave rectifying bridge and connected with the needle-plate discharge electrodes inside the gas reactor filled with pure CO_2. The gas is ionized, and the triboelectric plasma is generated when the output voltage reaches the discharge threshold voltage of CO_2 gas [36]. For a corona discharge, strong excitation and ionization exist near the needle surface with a high electric field strength, which is called the ionization zone. The region outside the ionization zone is called the migration zone, where the electric field intensity is not high enough to cause ionization, and the current conduction depends on the ion or electron migration (Fig. 1b).

A W needle and a Pt plate were used as the discharge electrodes with 2 mm distance and 200 rpm TENG rotational speed; thus, the electrical curves and the CO_2 decomposition properties were measured and shown in Fig. 1c and d, respectively. The open-circuit voltage of the TENG reached 4.5 kV (Fig. S2). As shown in Fig. 1c, when the potential difference between the needle-plate electrodes reached −0.8 kV, a discharge current with a peak of −10 μA and a duration of 45 ms occurred, indicating the triboelectric plasma generation in a negative corona discharge. Under this condition, CO_2 molecules were

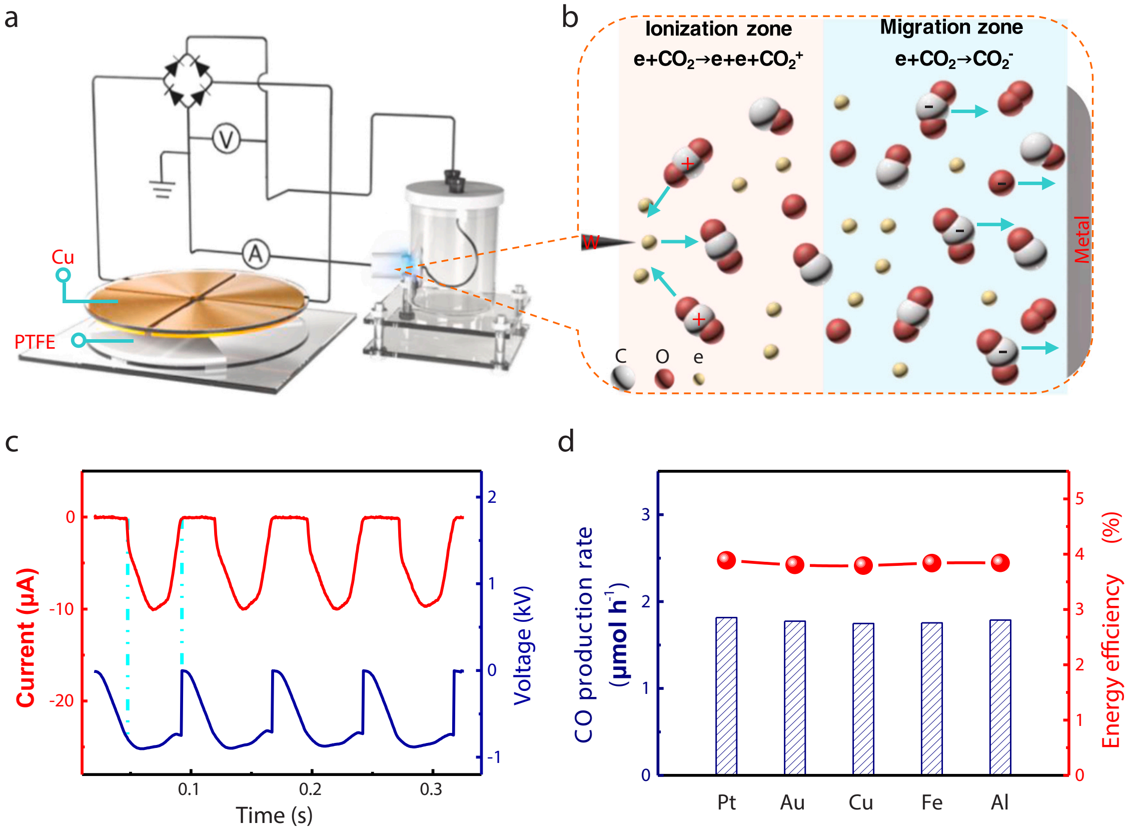

Fig. 1. Triboelectric plasma CO_2 decomposition driven by mechanical energy. (a) Schematic diagram of experimental device. (b) Diagram of CO_2 decomposition induced by triboelectric plasma. (c) Electrical curves of triboelectric plasma when Pt was plate electrode. (d) Activity and energy efficiency from electric energy to chemical energy of triboelectric plasma CO_2 decomposition. Reaction conditions: rotational speed: 200 rpm; needle-plate distance: 1.5 mm; reaction time: 1 h; room temperature and atmospheric pressure.

decomposed into CO with near 100% selectivity (Fig. S3), and the evaluation rate of CO (r_{CO}) measured by a gas chromatograph (Agilent GC7980) reached 1.8 μmol h^{-1}. Isotope labeling experiments verified that the CO gas comes from the reaction gas of CO_2, but not from the pollutant gas in the CO_2 gas or the environment (Fig. S4). The energy efficiency ($\eta_{ele-chem}$) from electric energy to chemical energy of triboelectric plasma CO_2 decomposition is estimated as follows (1):

$$\eta_{ele-chem} = \frac{r_{CO} \cdot \Delta H_R}{P_{ave}} \tag{1}$$

where, ΔH_R is the reaction enthalpy of CO_2 splitting to CO ($279.8 kJ \cdot mol^{-1}$), and P_{ave} is the average power of triboelectric plasma expressed as:

$$P_{ave} = \frac{\int_0^t V \cdot I \cdot dt}{t} \tag{2}$$

From integrating the measured voltage and the current curves of triboelectric plasma in 3 h, P_{ave} was calculated as 3.6 mW. Using the measured r_{CO} value of 1.8 μmol h^{-1}, a $\eta_{ele-chem}$ value of 3.8% was achieved.

Subsequently, the CO_2 decomposition properties were measured and plotted in Fig. 1d. The other metal materials (i.e. Au, Cu, Fe, and Al) were used as the plate electrodes. Similar electrical curves were obtained for different metal plate electrodes (Figs. S5 and S6). The measured values of P_{ave} (3.5–3.6 mW), r_{CO} (1.7–1.8 μmol h^{-1}), and $\eta_{ele-chem}$ (3.8–3.9%) were almost the same as Pt was used as the plate electrode. These experimental results show that the CO_2 decomposition is mainly driven by the triboelectric plasma, and the plate electrode materials do not significantly affect the CO_2 decomposition properties. Hence, in the following experiments, Pt was chosen as the plate electrode to study the effects of the triboelectric plasma on the CO_2 decomposition. Moreover, 200 rpm was chosen as the rotational speed, as the energy efficiency at 200 rpm rotational speed was the highest among the different rotational speeds (Fig. S7).

2.2. *Influence of the d and corona polarity on the CO_2 decomposition performances*

The ***d*** and the polarity of the corona discharge play an important role in the triboelectric plasma characteristics. The polarity of the corona discharge depends on the polarity of the W needle, and a positive/negative corona should be produced as the W needle connects with the positive/negative terminal of the rectifying bridge [37]. Fig. 2a–d show the electrical and CO_2 decomposition properties of triboelectric plasma with various ***d*** (1.5, 2.5, and 3.5 mm). First, the case of the negative corona is discussed as an example. The discharge voltage decreased (Fig. 2a), while the discharge current increased (Fig. 2b) as ***d*** dropped from 3.5 mm to 1.5 mm. According to Eq. (2), P_{ave} was calculated by integrating the product of the discharge voltage and the discharge current over time, which slowly increased with the decrease of ***d*** (Fig. 2c). The driving force of CO_2 decomposition was provided from the triboelectric plasma; thus, the measured r_{CO} increased with the increase in P_{ave} (Fig. 2c). Moreover, a beyond-linear growth trend was observed between r_{CO} and P_{ave}, causing an increased $\eta_{ele-chem}$ with a reduced ***d*** (Fig. 2d). As for the case of the positive corona, the trend of the discharge voltage, discharge current, P_{ave}, r_{CO}, and $\eta_{ele-chem}$ with ***d*** was the same as that of the negative corona. ***d*** was 1.5 mm; thus, the r_{CO} and $\eta_{ele-chem}$ of both the negative and positive corona discharges reached the optimal value.

Next, the effect of polarity on the CO_2 decomposition was investigated. ***d*** was 1.5 mm; therefore, the absolute value of the discharge voltage of the negative corona (0.80 kV) was lower than that of the positive corona (1.45 kV), and the absolute value of the discharge current of the negative corona (10.5 μA) was higher than that of the positive corona (9.8 μA). P_{ave} of the negative corona was 3.6 mW, which was less

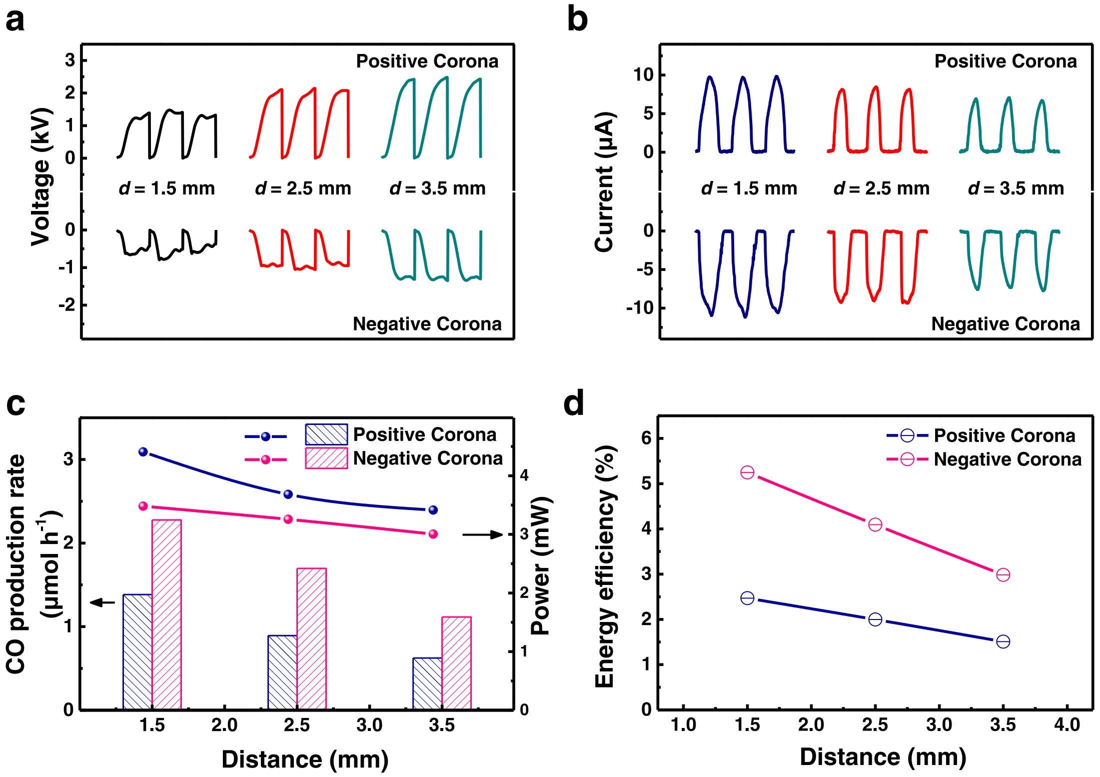

Fig. 2. Influence of the discharge polarity on the CO_2 decomposition performance at 200 rpm rotational speed. (a) Voltage curves of positive and negative corona. (b) Current curves of positive and negative corona. (c) CO_2 decomposition activities and discharge power in the positive and negative corona. (d) Energy efficiencies from electric energy to chemical energy of positive and negative corona.

than that of the positive corona (4.4 mW). However, r_{CO} of the negative corona with a lower P_{ave} (2.2 μmol h^{-1}) was 1.7 times of the positive corona (1.3 μmol h^{-1}), resulting in the higher $\eta_{ele-chem}$ for the negative corona. Hence, the $\eta_{ele-chem}$ of the negative corona (5.2%) was 2.2 times of the positive corona (2.4%). A similar phenomenon was also obtained considering that $\boldsymbol{d}$ was 2.5 and 3.5 mm. The aforementioned results demonstrated that the negative corona with a lower P_{ave} exhibited a superior activity and an energy efficiency of CO_2 decomposition at the same $\boldsymbol{d}$.

2.3. Detection and theoretical calculation of the reactive species CO_2^-

Using a 5,5-dimethyl-1-pyrroline-N-oxide (DMPO) solution as a capture reagent, the spin-trapped technology was used to investigate the derived reactive species from the CO_2 decomposition at different discharge polarities. Under the negative corona, a complex and overlapping multiple-peak signal occurred in the EPR spectrum, (Fig. 3a (I)). Through computer fitting and peak splitting, this signal was decomposed into a 1:2:2:1 (ratio of the peak relative intensity) quartet peaks (II) and a 1:1:1:1:1:1 sextet peaks (III) [38,39]. For the quartet peaks, $\alpha^N = \alpha^H_\beta = 15.0$ G, which was assigned to DMPO-OH. Here, α^N and α^H_β are the hyperfine coupling constant of N and H spin in DMPO-OH, respectively. For the sextet peaks, $\alpha^N = 15.8$ G and $\alpha^H_\beta = 19.1$ G, which was assigned to DMPO-CO_2^-. In a comparison of the positive corona shown in Fig. 3b, only the characteristic quartet peaks of DMPO-OH were observed, and no characteristic sextet spectrum of DMPO-CO_2^- appeared. These results unambiguously demonstrate that CO_2^- radicals with high reactivity were only formed in the negative corona, which may be the essential prerequisite for the enhanced activity and energy efficiency of the CO_2 decomposition in the negative corona. In addition, in both discharge polarities, the observed DMPO-OH was derived from the dissociation of the H_2O molecules in the DMPO solution, and no·OH radicals could be formed in the process of the triboelectric plasma CO_2 decomposition under a pure CO_2 atmosphere.

The single-point potential energy curves (PEC) of the CO_2 molecules and the CO_2^- anions were calculated using the theory of CCSD(T) levels to illustrate the effect of the CO_2^- reactive species on the CO_2 decomposition [40,41]. Fig. 3c shows the PECs of the CO_2 molecules and the CO_2^- anions as a function of the O═C═O bond angle. When the O═C═O bond angle was 180°, the potential energy of the free CO_2^- anions in the gas was 0.8 eV higher than that of the neutral CO_2 molecules. This process can be expressed in Eq. (3), in which the minimum energy of 0.8 eV is required because the ground state CO_2 molecules are excited into the CO_2^- anions.

$$e + CO_2 \rightarrow CO_2^- \tag{3}$$

The O═C═O bond angle of the CO_2^- anions was 135°; hence, it had the lowest energy and the most stable configuration. The results revealed that linear CO_2 molecules are first excited into the linear CO_2^- anions by electrons, which subsequently relaxed into a more stable curved geometry via asymmetric stretching and bending vibrations. The curved CO_2^- species had a certain lifetime of approximately 50–90 μs in the gas phase [42].

Fig. 3d shows the PECs of the CO_2^- anions and the CO_2 molecules as a function of the O═C═O bond length. The required minimum energy was 3.9 eV because the CO_2^- anions were decomposed into the CO and O^- anions (Eq. 4).

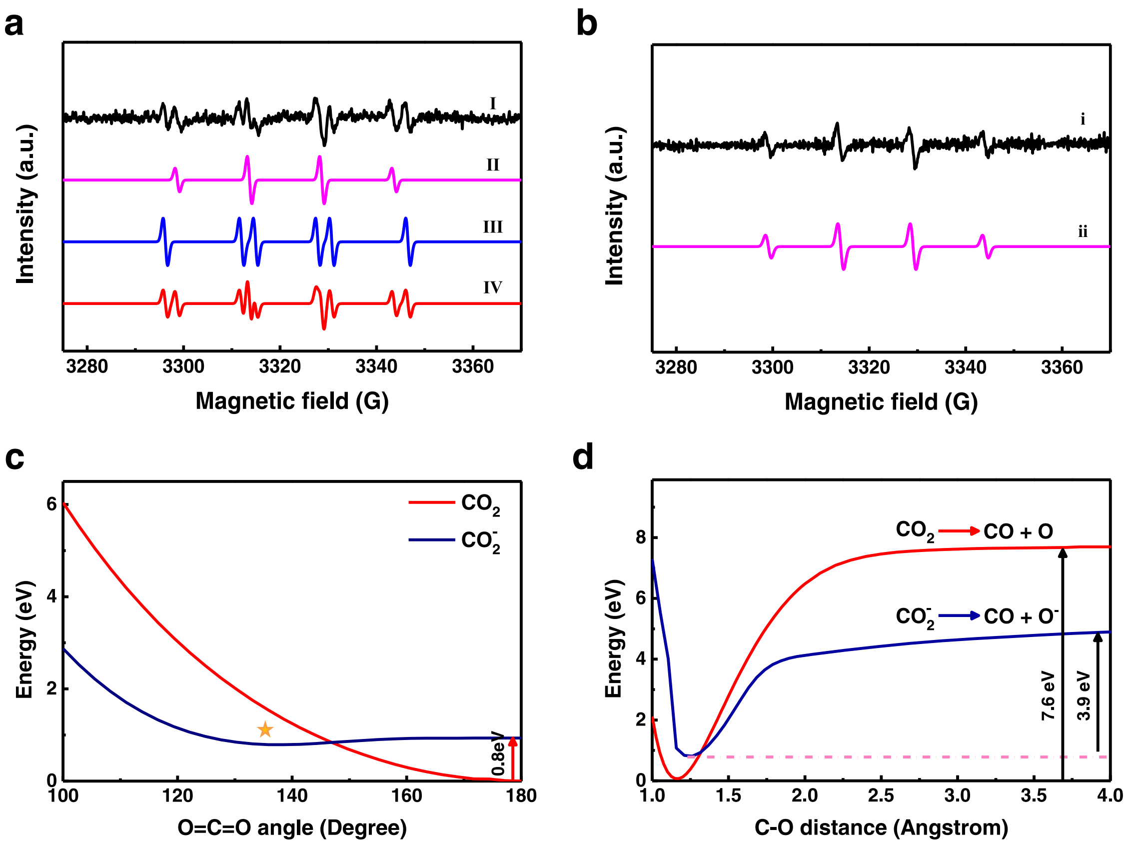

Fig. 3. Detection and theoretical calculation of the CO_2-derived reactive species in the triboelectric plasma. (a) Electron paramagnetic resonance (EPR) spectra of the reactive species in the negative corona, where curves I–IV are the EPR spectra in the negative corona, simulated EPR spectra of DMPO-OH, simulated EPR spectra of DMPO−CO_2, and simulated sum of EPR spectra, respectively. (b) EPR spectra of the reactive species in the positive corona, where curves i and ii are the EPR spectra in the positive corona and the simulated EPR spectra, respectively. (c) Potential energy curves (PECs) of the CO_2 and CO_2^- anions as a function of the O═C═O bond angle, where the asterisk indicates the equilibrium state. (d) PECs of the CO_2 and CO_2^- anions as a function of the C—O bond length.

$$CO_2^- \to CO + O^- \tag{4}$$

The CO_2 molecules were directly decomposed into CO and O atoms (Eq. 5); thus, the required minimum energy was 7.6 eV, which is consistent with the results in the previous literature [29].

$$CO_2 \to CO + O \tag{5}$$

According to above calculation results, the CO_2 decomposition has two different pathways. The first pathway is defined as the electron attachment dissociation (EAD) process, in which the electrons are first captured by the electronegative CO_2 molecules to form the reactive species CO_2^- anions (Eq. 3), and the CO_2^- anions are dissociated into CO and O^- anions (Eq. 4) [29,31,32]. The second pathway is defined as the electron collision dissociation (EID) process, in which the CO_2 molecules are directly dissociated into CO and O atoms by the electron collision [40,42]. As the CO_2^- anions are formed, the frequency of the stretching vibration of the O = C = O chemical bond is greatly weakened, making the bond dissociation easier [42]. Therefore, the minimum energy required for the CO_2^- anion dissociation in the EAD pathway is 3.7 eV lower than that of the EID pathway, making the EAD pathway more advantageous in terms of thermodynamics.

2.4. Simulation of electron density and energy distribution of triboelectric plasma

In the triboelectric plasma, the electron density and the electron energy greatly influence the reaction pathway for the CO_2 decomposition, but they are not easy to measure from the experiment. Therefore, the computer simulations were performed for a better understanding of the CO_2 decomposition process. Fig. 4a and b show the simulated time evolution mapping of the electron density and the electron average energy as the negative corona discharge was driven by a TENG at a ***d*** of 1.5 mm (see SI for details). With the increase of time, the electrons gradually diffused from the W tip to the plate electrode, and a hemispherical plasma channel with 1.5 mm radius was formed at 30 ns. Both the electron density and the average electron energy in the hemispherical plasma channel gradually decreased with the increase of the distance from the W tip. For example, the electron density and the average

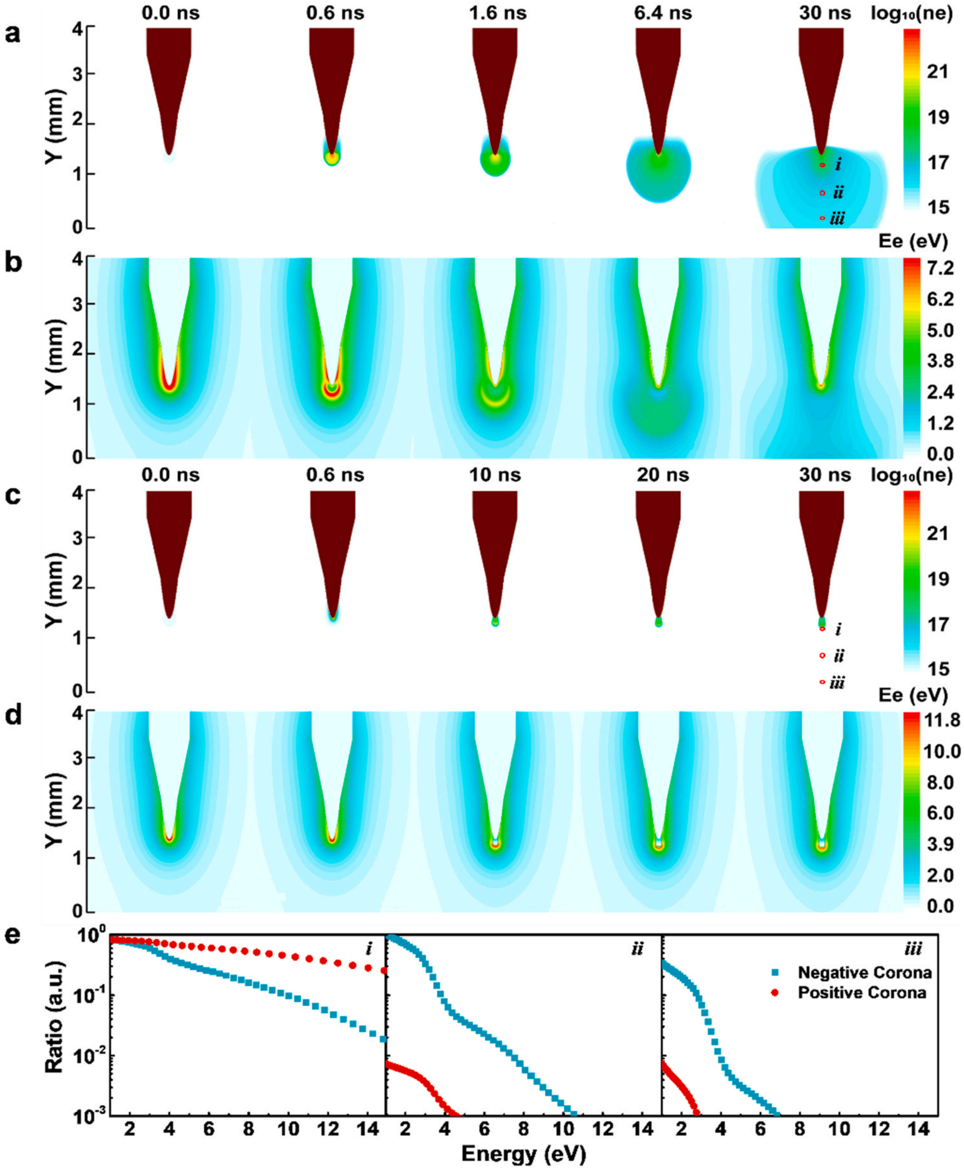

Fig. 4. Triboelectric plasma simulation. (a) Time evolution of the electron density distribution in the negative corona. (b) Time evolution of the electron energy distribution in the negative corona. (c) Time evolution of the electron density distribution in the positive corona. (d) Time evolution of the electron energy distribution in the positive corona. (e) Electron energy distribution function (EEDF) of three representative points both in the negative and positive corona.

electron energy around the W tip were approximately 1.0 × 10^{18} m^{-3} and 7.5 eV, and the corresponding values around the plate electrode were approximately 1.0 × 10^{17} m^{-3} and 1.5 eV, respectively.

Fig. 4c and d depict the time evolution of the electron density and the electron average energy for the positive corona. As time passed, the electrons were only concentrated near the tip of the W needle. At 30 ns, an elliptical region with a radius of only 0.2 mm was formed around the tip. The electron density and the average electron energy in the tip–plate gap remarkably decreased beyond the distance of 0.2 mm from the W tip. The electron density and the average electron energy near the W tip were approximately 1.3 × 10^{18} m^{-3} and 11.5 eV, respectively. However, the two values near the plate electrode were 1.0 × 10^{15} m^{-3} and 2.0 eV, respectively.

The normalized electron energy distribution function (EEDF) of the negative and positive corona at three representative points was calculated and plotted in Fig. 4e to gain insight into the electron energy distribution in the plasma channel. As marked in Fig. 4a and c, the distances from points *i* to *iii* to the W tip were 0.2, 0.8, and 1.3 mm, respectively. These curves show that the average electron energy at point *i* was remarkably higher than that at points *ii* and *iii*. For example, at point *i*, the energy of 19% electrons for the negative corona and 42% electrons for the positive corona was higher than 7.6 eV. However, at points *ii* and *iii*, almost all the electrons for both the negative and positive corona had an energy lower than 7.6 eV. In addition, for points *ii* and *iii* far away from the W tip under the positive corona, the electron density sharply decreased, which was approximately three orders of magnitude lower than that of point *i* near the W tip.

2.5. The dissociation pathways and efficiency of CO_2 decomposition

Fig. 5 depicts the proposed schematic diagrams of the two dissociation pathways of CO_2: EAD and EID processes. The EAD process of CO_2 has two dissociation steps: (1) the CO_2^- anion is formed in the first step with a required energy of 0.8 eV, and (2) the CO_2^- anion is dissociated into CO and O^- anions in the second step with a required energy of 3.9 eV. The total energy consumed in an entire EAD process was 4.7 eV. In the EID process of CO_2, CO_2 was directly dissociated into CO and O atoms in only one step, but the consumed energy of this step was as high as 7.6 eV, which was 2.9 eV higher than the total consumed energy of the EAD process. Therefore, the EAD process of the CO_2 decomposition required a lower energy, resulting in a higher energy efficiency compared to the EID process. Furthermore, the reaction rate coefficient of the EAD process at the same electron density was greater than that of the EID process when the average electron energy of the triboelectric plasma was below 4.0 eV (Fig. S8).

The above discussions revealed two dissociation pathways of CO_2 determined by the spatial and energy distributions of electrons in the triboelectric plasma. In the negative corona, the electrons were evenly distributed in the gap between the W tip and the plate electrodes (Fig. 4a). Except for the electrons near the W tip, most electrons in the other regions had an energy less than 7.6 eV (Fig. 4b and e), which did not have enough energy for the EID process. Hence, the CO_2 decomposition was mainly dominated by the EAD process, which only occurs around the W tip with a low proportion. In the case of the positive corona, almost all electrons were distributed near the W tip, and approximately 42% electrons had an energy higher than 7.6 eV in such region (Fig. 4c–e). Therefore, both the EAD and EID processes are the major pathways of the CO_2 decomposition. Consequently, the EAD process proportion in the negative corona was remarkably higher than that in the positive corona, causing the higher activity and energy efficiency of the CO_2 decomposition in the former. As discussed in Fig. 2, the activity and the energy efficiency for both negative and positive corona increased as ***d*** decreased. At a shorter distance, the inception voltage of the corona discharge was decreased (Fig. 2a), which was considered to decrease the average electron energy of the triboelectric plasma. Thus, the EAD process proportion in the CO_2 decomposition increased, increasing the activity and the energy efficiency of the CO_2 decomposition.

In this experiment, the maximum energy efficiency from electric energy to chemical energy of CO_2 decomposition driven by triboelectric plasma in the negative corona discharge was 5.2%. However, the selectivity of triboelectric plasma CO_2 decomposition into CO was near 100%, which was much higher than that (50–80%) of traditional corona discharge systems (Table S1). The traditional plasma system uses a sophisticated reaction device and a precision control circuit, and its driven energy mainly comes from the thermal power generation. Compared with the traditional plasma system, triboelectric plasma system has the advantages of broad material sources, lightweight structure, cheap production, and easy utilization in a wide range. The energy efficiency ($\eta_{mech-chem}$) from mechanical energy to chemical energy of this system was calculated as the following Eq. (6):

$$\eta_{mech-chem} = \eta_{mech-ele} \times \eta_{ele-chem} \tag{6}$$

According to the literature, the energy efficiency ($\eta_{mech-ele}$) of this mode TENG from mechanical energy to electrical energy was 24% [43]. Using the calculated $\eta_{ele-chem}$ (5.2%) of triboelectric plasma system, the $\eta_{mech-chem}$ was calculated to be 1.2%, which was approximately one orders of magnitude higher than that of wave-energy-driven electrochemical CO_2 reduction system (0.5‰) [44]. The lower energy efficiency of wave-energy-driven electrochemical CO_2 reduction system is possibly attributed to the mismatch between the internal impedance (~MΩ) of TENG and the electrochemical cell (~Ω), resulting in the

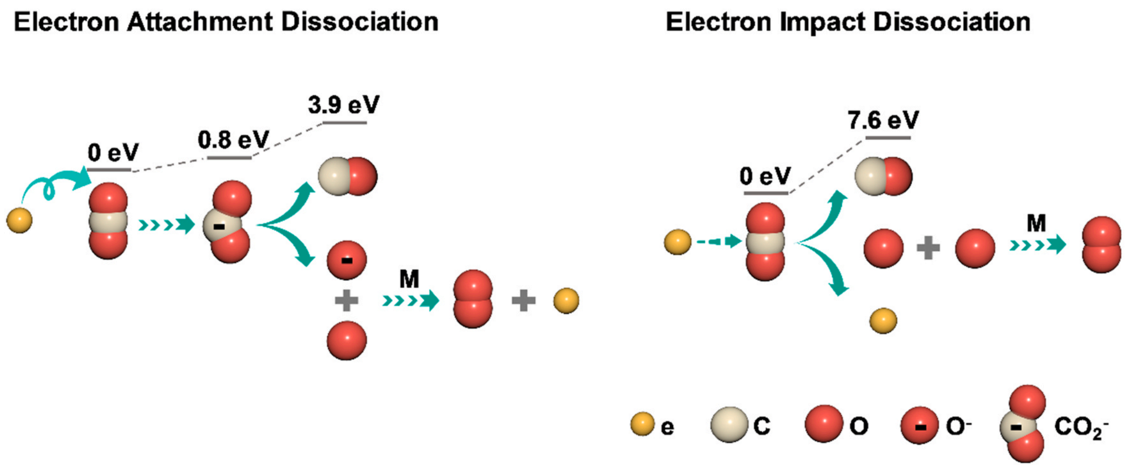

Fig. 5. Diagrams of the two dissociation pathways for the triboelectric plasma CO_2 decomposition.

difficulty of transfer of energy from the wave energy to the electrochemical cell and the poor energy efficiency of overall system [44]. However, the triboelectric plasma could effectively reduce the impedance of TENG, effectively solving the problem of the impedance mismatch and hence increasing the overall energy efficiency [36]. Clearly, the triboelectric plasma system recorded by far the highest energy efficiency among the mechanical energy-driven CO_2 reduction systems (Table S2) [44]. It can also directly utilize random mechanical energy, which is widely distributed and not effectively utilized in nature. As a demonstration, the triboelectric plasma decomposition system could use the breeze to decompose CO_2, and a CO evaluation rate of 0.6 μmol h^{-1} has been achieved at a wind speed of 4.7 m s^{-1} (Fig. S9). TENG could collect wind energy, water energy from the environment or kinetic energy wasted in the factory to reduce CO_2 in the exhaust gas produced during the generation process of thermal power.

3. Conclusion

In summary, a TENG-based triboelectric plasma decomposition system was constructed, which utilized cheap and ubiquitous mechanical energy to decompose CO_2 to CO with near 100% selectivity at normal temperature and pressure. In this system, the high-voltage electrical output of the TENG could break down gases and generate the triboelectric plasma. Under the negative corona, the record energy efficiency from the mechanical energy to chemical energy of the system was up to 1.2%. The electrons in the triboelectric plasma were directly transferred into the anti-bonding state of the CO_2 molecules, forming numerous highly reactive CO_2^- species. Compared with the direct dissociation of the CO_2 process, the energy barrier for the CO_2^- anion decomposition via the EAD process was lowered by 3.7 eV, which effectively boosted the CO_2 dissociation. Finally, the triboelectric plasma CO_2 decomposition system could effectively convert greenhouse gases under mechanical energy stimulation in external environments. The system had the advantages of being lightweight, simple structure, low cost, easy operation, and convenient application. This study provides a new strategy of using renewable mechanical energy to convert CO_2 into high value-added chemicals.

Declaration of Competing Interest

The authors declare that they have no known competing financial interests or personal relationships that could have appeared to influence the work reported in this paper.

Acknowledgements

The funding from the National Natural Science Foundation of China (61974040, 21902043, 22005086), the Leading Talents of Scientific and Technological Innovation in Central Plains Thousand People Programme (194200510004), China Postdoctoral Science Foundation (2020M672197), and Key Research & Development and Promotion Project of Henan Province (Science and Technology Tackling Key Problems, 212102311004) are appreciated. We thanked Dr. Xianwen Zhang and Prof. Can Li at State Key Laboratory of Catalysis, Dalian Institute of Chemical Physics, Chinese Academy of Sciences for the EPR experiments.

Appendix A. Supporting information

Supplementary data associated with this article can be found in the online version at doi:10.1016/j.nanoen.2021.106287.

References

[1] C.W. Zhu, K. Kobayashi, I. Loladze, J.G. Zhu, Q. Jiang, X. Xu, G. Liu, S. Seneweera, K.L. Ebi, A. Drewnowski, N.K. Fukagawa, L.H. Ziska, Sci. Adv. 4 (2018), eaaq1012, https://doi.org/10.1126/sciadv.aaq1012.

[2] G. Tamburello, S. Pondrelli, G. Chiodini, D. Rouwet, Nat. Commun. 9 (2018) 4608–4617, https://doi.org/10.1038/s41467-018-07087-z.

[3] M.T. Tang, H. Peng, P.S. Lamoureux, M. Bajdich, F.A. Pedersen, Appl. Catal. B 279 (2020), 119384, https://doi.org/10.1016/j.apcatb.2020.119384.

[4] S.H. Kim, K.H. Kim, S.H. Hong, Angew. Chem. Int. Ed. 53 (2014) 771–774, https://doi.org/10.1002/anie.201308341.

[5] J. Wei, Q.J. Ge, R.W. Yao, Z.Y. Wen, C.Y. Fang, L.S. Guo, H.Y. Xu, J. Sun, Nat. Commun. 8 (2017) 15174, https://doi.org/10.1038/ncomms15174.

[6] R. Aerts, W. Somers, A. Bogaerts, ChemSusChem 8 (2015) 702–716, https://doi.org/10.1002/cssc.201402818.

[7] A.W. Kleij, M. North, A. Urakawa, ChemSusChem 10 (2017) 1036–1038, https://doi.org/10.1002/cssc.201700218.

[8] Q.W. Song, Z.H. Zhou, L.N. He, Green Chem. 19 (2017) 3707–3728, https://doi.org/10.1039/c7gc00199a.

[9] M.D. Porosoff, B. Yan, J.G. Chen, Energy Environ. Sci. 9 (2016) 62–73, https://doi.org/10.1039/c5ee02657a.

[10] D.D. Zhu, J.L. Liu, S.Z. Qiao, Adv. Mater. 28 (2016) 3423–3452, https://doi.org/10.1002/adma.201504766.

[11] K. Li, B. Peng, T. Peng, ACS Catal. 6 (2016) 7485–7527, https://doi.org/10.1021/acscatal.6b02089.

[12] J. Wang, Y. Zi, S. Li, X. Chen, MRS Energy Sustain. 6 (2020) 1–23, https://doi.org/10.1557/mre.2020.2.

[13] H.M. Naimi, S.V. Zadeh, Energy Policy 43 (2012) 351–361, https://doi.org/10.1016/j.enpol.2012.01.012.

[14] Y. Wang, J. Liu, Y. Wang, Y. Wang, G. Zheng, Nat. Commun. 9 (2018) 5003, https://doi.org/10.1038/s41467-018-07380-x.

[15] S. Park, J. Park, Y.G. Kim, S. Bae, T.W. Kim, K.I. Park, B.H. Hong, C.K. Jeong, S. K. Lee, Nano Energy 78 (2020), 105266, https://doi.org/10.1016/j.nanoen.2020.105266.

[16] K. Zhao, Y. Yang, X. Liu, Z.L. Wang, Adv. Energy Mater. 7 (2017), 1700103, https://doi.org/10.1002/aenm.201700103.

[17] T. Quan, Y. Wu, Y. Yang, Nano Res. 8 (2015) 3272–3280, https://doi.org/10.1007/s12274-015-0827-6.

[18] T. Quan, Y. Yang, Nano Res. 9 (2016) 2226–2233, https://doi.org/10.1007/s12274-016-1109-7.

[19] L. Lin, S. Wang, S. Niu, C. Liu, Y. Xie, Z.L. Wang, Adv. Mater. 6 (2014) 3031–3038, https://doi.org/10.1021/am405637s.

[20] Z.L. Wang, Faraday Discuss. 176 (2014) 447–458, https://doi.org/10.1039/c4fd00159a.

[21] A. Ahmed, I. Hassan, A.S. Helal, V. Sencadas, A. Radhi, C.K. Jeong, M.F. El-Kady, iScience 23 (2020), 101286, https://doi.org/10.1016/j.isci.2020.101286.

[22] X. Liu, K. Zhao, Z.L. Wang, Y. Yang, Adv. Energy Mater. 7 (2017), 1701629, https://doi.org/10.1002/aenm.201701629.

[23] Y. Yang, H. Zhang, Z.L. Wang, Adv. Funct. Mater. 24 (2014) 3745–3750, https://doi.org/10.1002/adfm.201304295.

[24] J. Cheng, W.B. Ding, Y.L. Zi, Y.J. Liu, F. Liu, C.S. Wu, Z.L. Wang, Nat. Commun. 9 (2018) 3733, https://doi.org/10.1038/s41467-018-06198-x.

[25] F. Liu, Y. Liu, Y.J. Liu, Z.Z. Wang, Y.X. Shi, L.H. Ji, J. Cheng, Nano Energy 56 (2019) 482–493, https://doi.org/10.1016/j.nanoen.2018.11.064.

[26] S.G.R. Hawtof, E. Guarr, C.Y. Xu, R.M. Sankaran, J.N. Renner, Sci. Adv. 5 (2019), eaat5778, https://doi.org/10.1126/sciadv.aat5778.

[27] Y. Su, Y. Yang, X. Zhong, H. Zhang, Z. Wu, Y. Jiang, Z.L. Wang, ACS Appl. Mater. Interfaces 6 (2014) 553–559, https://doi.org/10.1021/am404611h.

[28] H. Wang, Z. Xiang, P. Giorgia, X. Mu, Y. Yang, Z.L. Wang, C. Lee, Nano Energy 23 (2016) 80–88, https://doi.org/10.1016/j.nanoen.2016.02.054.

[29] M. Ramakers, G. Trenchev, S. Heijkers, W.Z. Wang, A. Bogaerts, ChemSusChem 10 (2017) 11–15, https://doi.org/10.1002/10.1002/cssc.201700589.

[30] A. Lebouvier, S.A. Iwarere, P. d Argenlieu, D. Ramjugernath, L. Fulcheri, Energy Fuels 27 (2013) 2712–2722, https://doi.org/10.1021/ef301991d.

[31] A. Bogaerts, E.C. Neyts, ACS Energy Lett. 3 (2018) 1013–1027, https://doi.org/10.1021/acsenergylett.8b00184.

[32] R. Snoeckx, A. Bogaerts, Chem. Soc. Rev. 46 (2017) 5805–5863, https://doi.org/10.1039/c6cs00066e.

[33] M.C. Wong, W. Xu, J. Hao, Adv. Funct. Mater. 29 (2019), 1904090, https://doi.org/10.1002/adfm.201904090.

[34] K. Han, J.J. Luo, Y.W. Feng, L. Xu, W. Tang, Z.L. Wang, Energy Environ. Sci. 13 (2020) 2450–2458, https://doi.org/10.1039/d0ee01102a.

[35] F. Yang, J.M. Guo, L. Zhao, W.Y. Shang, Y.Y. Gao, S. Zhang, G.Q. Gu, B. Zhang, P. Cui, G. Cheng, Z.L. Du, Nano Energy 67 (2020), 104210, https://doi.org/10.1016/j.nanoen.2019.104210.

[36] K. Zhao, G.Q. Gu, Y.N. Zhang, B. Zhang, F. Yang, L. Zhao, M.L. Zheng, G. Cheng, Z. L. Du, Nano Energy 53 (2018) 898–905, https://doi.org/10.1016/j.nanoen.2018.09.057.

[37] J.D. Skalny, A. Stoica, J. Orszagh, R. Vladoiu, N.J. Mason, J. Phys. D Appl. Phys. 41 (2008), 175211, https://doi.org/10.1088/0022-3727/41/17/175211.

[38] E.J.L. Frederick, A. Villamena, A. Rockenbauer, C.M. Hadad, J.L. Zweier, J. Phys. Chem. A 110 (2006) 13253–13258, https://doi.org/10.1021/jp064892m.

[39] A.V. Taborda, M.A. Brusa, M.A. Grela, Appl. Catal., A 208 (2001) 419–426, https://doi.org/10.1016/S0926-860X(00)00727-4.

[40] G.L. Gutsev, R.J. Bartlett, J. Chem. Phys. 108 (1998) 6756–6763, https://doi.org/10.1063/1.476091.

[41] T.B. Adler, G. Knizia, H.J. Werner, J. Chem. Phys. 127 (2007), 221106, https://doi.org/10.1063/1.2817618.
[42] D. Schröder, C.A. Schalley, J.N. Harvey, H. Schwarz, Int. J. Mass Spectrom. 185–187 (1999) 25–35, https://doi.org/10.1016/S1387-3806(98)14042-3.
[43] G. Zhu, J. Chen, T.J. Zhang, Q.J. Jing, Z.L. Wang, Nat. Commun. 5 (2014) 3426, https://doi.org/10.1038/ncomms4426.
[44] S.F. Leung, H.C. Fu, M. Zhang, A.H. Hassan, T. Jiang, K.N. Salama, Z.L. Wang, J. H. He, Energy Environ. Sci. 13 (2020) 1300–1308, https://doi.org/10.1039/c9ee03566d.

Sumin Li received the M.D. degree from Shaanxi University of Science & Technology, China, in 2007. She is currently a Ph.D. candidate in the Key Lab of Ministry of Education for Special Functional Materials of Henan University. Her research interests are triboelectric nanogenerator driven discharge plasma and applications of triboelectric plasma in the energy conversion & environment.

Bao Zhang is a lecturer of Key Lab for Special Functional Materials, Ministry of Education, Henan University. He received his Ph.D. degree from Dalian Institute of Chemical Physics under the supervision of Prof. Can Li, Chinese Academy of Sciences. His research interests include the application of triboelectric nanogenerators in environment and energy.

Guangqin Gu received the B.S. degree from Henan University in 2012 and the Ph.D. degree from Beijing Institute of Nanoenergy and Nanosystems, University of Chinese Academy of Sciences, under the supervision of Prof. Zhong Lin Wang in 2018. Currently, he is a lecturer at the Key Lab for Special Functional Materials, Ministry of Education, Henan University, Kaifeng, China. His research interests are triboelectric nanogenerator, TENG driven air discharge, and self-powered sensors and systems.

Xiaochen Xiang is currently pursuing the master degree at the Key Lab for Special Functional Materials, Ministry of Education, Henan University, Kaifeng, China. Her research interest are triboelectric plasma catalysis and catalyst optimization.

Wenhe Zhang is currently pursuing the master degree at the Key Lab for Special Functional Materials, Ministry of Education, Henan University, Kaifeng, China. His research interests are self-powered sensing system and applications of the triboelectric nanogenerator.

Xue Shi is a Ph.D. candidate at the Beijing Institute of Nanoenergy and Nanosystems, Chinese Academy of Sciences. Her research interest is self-powered sensors based on triboelectricity.

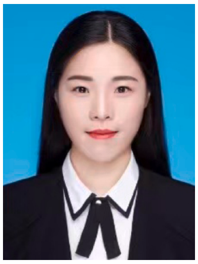

Ke Zhao received her M.S. in Materials Science and Engineering from Henan University in 2019. She is currently pursuing her Ph.D. degree in Chemistry at Chongqing University. Her research interest is electrochemical synthesis of nanomaterials for electrocatalysis.

Yifei Zhu received the B.S. degree from Airforce Engineering University in 2011 and the Ph.D. degree from Ecole Polytechnique (Paris Saclay) under the supervision of Prof. Starikovskaia Svetlana in 2018. Currently he is a lecturer in Xi'an Jiaotong University. His research interests are the modeling and diagnostics of low temperature plasma and its applications.

Junmeng Guo received his B.S. degree from Henan University and the Ph.D. degree from Beijing Institute of Nanoenergy and Nanosystems, University of Chinese Academy of Sciences in 2018. Currently, he is a lecturer at the Key Lab for Special Functional Materials, Ministry of Education, Henan University, Kaifeng, China. His research interests are 2D nanomaterials fabrication and characteristics, TENG-driven air discharge, and self-powered nanosensors.

Peng Cui received the B.S. degree from Jilin University in 2009 and the Ph.D. degree from Sungkyunkwan University in 2015. He was a Research Fellow in School of Materials Science and Engineering at Nanyang Technological University under the supervision of Prof. Lee Pooi See. Currently, he is an Assistant Professor at the Key Lab for Special Functional Materials, Ministry of Education, School of Materials Science and Engineering, Henan University. His research interests are triboelectric nanogenerators and self-powered electronic devices.

Gang Cheng received the B.S. degree from Henan University in 2000 and the Ph.D. degree from Jilin University in 2008. He was a visiting scholar in School of Materials Science and Engineering at Georgia Institute of Technology under the supervision of Prof. Zhong Lin Wang from 2013 to 2016. Currently, he is a full-time professor at the Key Lab for Special Functional Materials, Ministry of Education, Henan University, Kaifeng, China. His research interests are nanostructure-based electronic and optoelectronic devices, nanogenerator, and self-powered nanosensors.

Zuliang Du received the Master's degree (1991) and Ph.D. degree (1999) in Condensed Matter Physics from Jilin University. Now, he is director of Key Lab for Special Functional Materials of Ministry of Education, Henan University. His major is condensed matter physics and materials and his main interest is concerned with the research of nanostructures materials and devices, photoelectric materials and molecule assembly. Up to date, there are more than 10 national-level research projects in total completed or being undertaken, including those from the National Key Projects for Basic Researches of China (973-Project), the National High-Tech Programmes of China (863-Programmes), and the projects from the National Natural Science Foundation of China (NSFC).